Monthly Notices
of the
ROYAL ASTRONOMICAL SOCIETY

MNRAS **456,** 4524–4532 (2016) doi:10.1093/mnras/stv2858

ExoMol molecular line lists – XIII. The spectrum of CaO

Sergei N. Yurchenko, Audra Blissett, Usama Asari, Marcus Vasilios, Christian Hill and Jonathan Tennyson★

Department of Physics and Astronomy, University College London, London WC1E 6BT, UK

Accepted 2015 December 1. Received 2015 November 29; in original form 2015 July 31

ABSTRACT

An accurate line list for calcium oxide is presented covering transitions between all bound ro-vibronic levels from the five lowest electronic states $X\,^1\Sigma^+$, $A'\,^1\Pi$, $A\,^1\Sigma^+$, $a\,^3\Pi$, and $b\,^3\Sigma^+$. The ro-vibronic energies and corresponding wavefunctions were obtained by solving the fully coupled Schrödinger equation. *Ab initio* potential energy, spin-orbit, and electronic angular momentum curves were refined by fitting to the experimental frequencies and experimentally derived energies available in the literature. Using our refined model we could (1) reassign the vibronic states for a large portion of the experimentally derived energies (van Groenendael A., Tudorie M., Focsa C., Pinchemel B., Bernath P. F., 2005, J. Mol. Spectrosc., 234, 255), (2) extended this list of energies to $J = 61$–118 and (3) suggest a new description of the resonances from the $A\,^1\Sigma^+$–$X\,^1\Sigma^+$ system. We used high level *ab initio* electric dipole moments reported previously (Khalil H., Brites V., Le Quere F., Leonard C., 2011, Chem. Phys., 386, 50) to compute the Einstein A coefficients. Our work is the first fully coupled description of this system. Our line list is the most complete catalogue of spectroscopic transitions available for $^{40}Ca^{16}O$ and is applicable for temperatures up to at least 5000 K. CaO has yet to be observed astronomically but its transitions are characterized by being particularly strong which should facilitate its detection. The CaO line list is made available in an electronic form as supplementary data to this article and at www.exomol.com.

Key words: molecular data – opacity – astronomical data bases: miscellaneous – planets and satellites: atmospheres – stars: low-mass.

1 INTRODUCTION

The discovery of candidate 'Lava planets', such as Corot-7b (Leger et al. 2009), Kepler-10b (Rouan et al. 2011) and 55 CnC e (Winn et al. 2011), which are thought to support day-side temperatures around 3000 K, has opened a completely new field of (exo-)planet spectroscopy. Theoretical studies have proposed possible formation mechanisms for these planets (Leitzinger et al. 2011), compositions for their hot atmospheres (Castan & Menou 2011; Schaefer, Lodders, & Fegley 2012) and their possible spectroscopic signatures (Ito et al. 2015). They are considered important targets for space telescopes wishing to perform spectroscopic characterization of their atmospheres (Tinetti et al. 2012, 2016; Samuel et al. 2014).

Calcium oxide, which is quicklime in its solid form, is a possible constituent of rocky type exoplanets where it should exist in a gaseous form at higher temperatures. However, to the best of our knowledge the CaO molecule has not yet been detected astronomically although it has been searched for in molecular clouds by Sakamoto et al. (1998). Hocking et al. (1979) estimated the flux-range for CaO absorption in stellar atmospheres and molecular clouds; this analysis has been extended to the atmosphere of exoplanet CoRoT-7b by Guenther et al. (2011) who suggest that the signature for CaO should be particularly strong.

The first experimental study of the gaseous hot CaO using discharge was performed by Child (1911). Brodersen (1932) performed an experimental study of the $A\,^1\Sigma^+$–$X\,^1\Sigma^+$ electronic system of CaO, which was later complemented and re-analysed in a series of experimental works by Lagerqvist and co-workers (Hultin & Lagerqvist 1950, 1951; Lagerqvist 1954; Lagerqvist & Huldt 1954a,b; Lagerqvist, Nilsson & Barrow 1957) and also in a theoretical work by Field (1974). A number of band heads from the $A\,^1\Sigma^+$–$X\,^1\Sigma^+$ system were reported experimentally by Brewer & Hauge (1968). Recently the $A\,^1\Sigma^+$–$X\,^1\Sigma^+$ electronic system was addressed by van Groenendael et al. (2005) in their comprehensive study with the high-resolution Fourier transform spectroscopy (FTS). The strong $A'\,^1\Pi$–$X\,^1\Sigma^+$ band was studied experimentally by Field, Capelle & Jones (1975) with a number of band heads corresponding to vibrationally excited states reported and by Focsa et al. (2000) where a large number of ro-vibronic transitions were assigned. Hocking et al. (1978) reported millimeter wave spectra of CaO and also attempted a search of CaO in stars and molecular clouds though without success. The hot infrared spectrum of CaO

★E-mail: j.tennyson@ucl.ac.uk

($X\,^1\Sigma^+ - X\,^1\Sigma^+$) was observed by Blom & Hedderich (1988) and Hedderich & Blom (1989).

The orange arc bands of CaO, which arise from transitions between excited triplet states were studied by Marks et al. (1982) and Plane & Nien (1991). Other experimental works on the electronic spectra of CaO include studies of the $c\,^3\Sigma^+ - a\,^3\Pi$ band using the sub-Doppler intermodulation spectroscopy by Norman et al. (1989), $B\,^1\Pi - b\,^3\Sigma^+$ bands by Baldwin & Field (1990b) and the green-band transitions of the $F\,^1\Pi - A'\,^1\Pi$ and $B\,^1\Pi - A'\,^1\Pi$ systems by Baldwin & Field (1990a) using the dispersed laser fluorescence spectroscopy (LFS); the $C'\,^1\Sigma^+ - A'\,^1\Pi$, $e\,^3\Sigma^- - a\,^3\Pi$ and $E\,^1\Sigma^- - A'\,^1\Pi$ bands using a combination of laser-induced fluorescence, resolved fluorescence, and optical double resonance techniques by Baldwin & Field (1989) and Baldwin et al. (1990). The electronic transition strengths of the $B\,^1\Pi - X$ and $C'\,^1\Sigma^+ - X\,^1\Sigma^+$ bands of CaO were determined by absorption measurements in a shock tube by Svyatkin, Kuznetsova & Kuzyakov (1980a,b).

Lifetimes of the $A\,^1\Sigma^+ - X\,^1\Sigma^+$ and orange arc bands were measured by Plane & Nien (1991), which provide a useful check for our *ab initio* transition dipoles and hence predicted intensities. Dissociation energies were obtained experimentally by Drowart, Verhaegen & Exsteen (1964) using mass spectroscopy and by Irvin & Dagdigian (1980) from chemiluminescence. On the *ab initio* side, Khalil et al. (2011, 2012) reported high-level *ab initio* studies of CaO including accurate potential energy curves (PECs), spin-orbit curves (SOCs), electronic angular momentum curves (EAMCs), dipole moment curves (DMCs), transition dipole moment curves (TDMCs) as well as different structural properties including the dissociation energies. These results provide the input to our nuclear motion calculations and are considered in detail below.

The aim of this work is to produce a molecular line list for calcium oxide, $^{40}Ca^{16}O$ (hereafter CaO), as part of the ExoMol project Tennyson & Yurchenko (2012). This line list is a catalogue of transitions required for modelling absorption/emission of the molecule in question. We use the *ab initio* curves by Khalil et al. (2011, 2012) and Leonard (private communication) covering the lowest five electronic states, $X\,^1\Sigma^+$, $A'\,^1\Pi$, $A\,^1\Sigma^+$, $a\,^3\Pi$, and $b\,^3\Sigma^+$. The *ab initio* PECs, SOCs, and EAMC were refined by fitting to the experimental energies and transition frequencies from the literature. The line list is used to simulate different spectra for a range of temperatures of CaO which we validate against experiment.

2 METHOD

We use the program DUO (Yurchenko et al. 2016) to solve the fully coupled Schrödinger equation for the lowest five electronic states of CaO. The details of the DUO methodology used for building accurate, empirical line lists for diatomic molecules has been extensively discussed elsewhere (Patrascu et al. 2014; Lodi, Yurchenko & Tennyson 2015; Patrascu, Tennyson & Yurchenko 2015; Yurchenko et al. 2016; Tennyson et al. 2016a). The initial PECs, SOCs, EAMCs used were taken from Khalil et al. (2011, 2012) and Leonard (private communication) and are shown in Figs 1, 2, and 3. These curves were obtained using the multireference configuration interaction (MRCI) calculations in conjunction with the aug-cc-pV5Z and cc-pCV5Z basis sets for O and Ca, respectively.

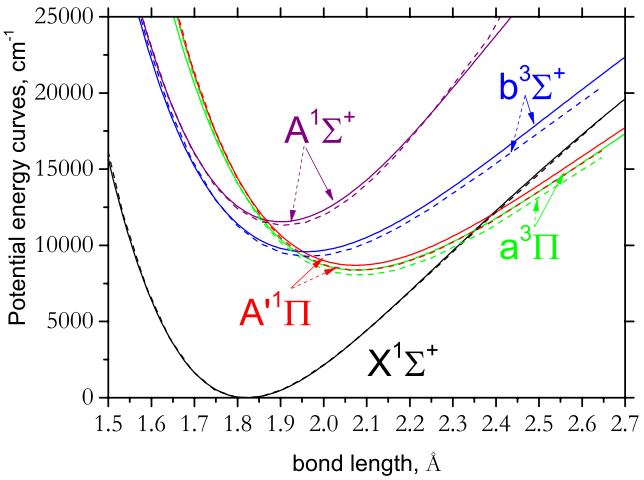

Figure 1. Ab initio (dotted curves) and fitted (full curves) potential energy curves for the lowest five electronic states of CaO.

Our DUO calculations used a grid-based sinc method with 501 points ranging from 1 to 4 Å to solve the five uncoupled vibrational eigenproblems for each state separately. The lowest 80 ($X\,^1\Sigma^+$) and 50 ($A\,^1\Sigma^+$, $A'\,^1\Pi$, $a\,^3\Pi$, and $b\,^3\Sigma^+$) vibrational eigenfunctions were then used as the vibrational basis functions for the ro-vibronic, fully coupled problem in a Hund's case (a) representation. This problem is solved variationally for each total angular momentum quantum number, J, and parity by explicit diagonalization of the coupled-states Hamiltonian.

3 EXPERIMENTAL DATA AND REFINEMENT

The *ab initio* PECs, SOCs, and EAMs were refined by fitting to the experientially derived energies and transition frequencies. This refinement used the same fitting approach as Patrascu et al. (2015).

The current status of the experiment spectroscopic data on the CaO is depicted in Table 1. Only the $a\,^3\Pi$ state dissociates to lowest products of O(^{3}P) and Ca(^{1}S); the other curves go asymptotically

Table 1. Sources and statistics of the experimental data for CaO used in this work as well as the number of energy levels extracted and their ranges. FTS = Fourier transform spectroscopy, LFS = laser fluorescence spectroscopy, SDIF = sub-Doppler intermodulated fluorescence, G = grating.

Source	Method	No. of levels	State	J	v	Energy range, cm^{-1}
Hultin & Lagerqvist (1950)	G	30	$A\,^1\Sigma^+$	2–119	0–6	15 995–17 264
van Groenendael et al. (2005)	FTS	210	$A\,^1\Sigma^+$	1–48	0–5	11 550–15 824
		73	$a^3\Pi_0$	2–60	6, 9,12	11 488–15 837
		32	$A'^1\Pi$	15–55	7,13	12 365–16 301
Focsa et al. (2000)[a]	FTS	531	$A'^1\Pi$	1–78	0,1,2,3	8608–11 219
		522	$X^1\Sigma^+$	0–77	0–7	0–6051
Norman et al. (1989)	SDIF	414	$a^3\Pi$	0–69	0–0	8349–9999
Baldwin & Field (1990b)	LIF	12	$b^3\Sigma^+$	14–25	1	10 178–10 354
Baldwin & Field (1990b)	LIF	12	$a^3\Pi$	14–25	3	10 016–10 164.1

Note. [a]Derived from 3018 $A\,^1\Sigma^+ - X\,^1\Sigma^+$ transition frequencies using combination differences.

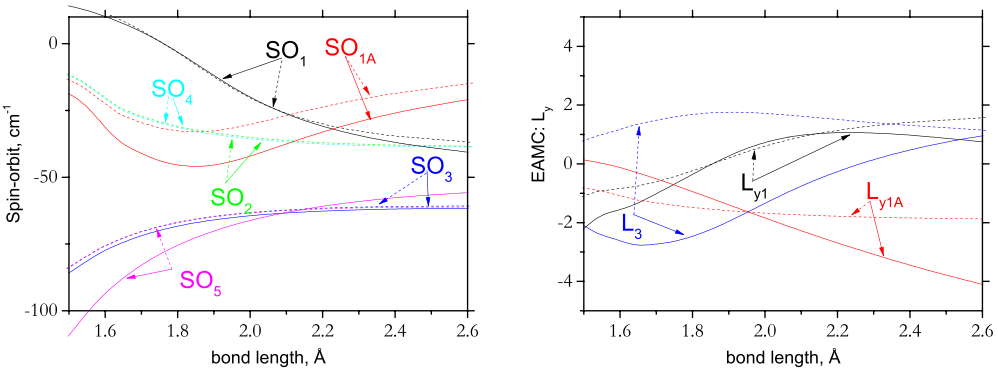

Figure 2. Ab initio (dotted curves) and fitted (full curves) spin-orbit (left) and electronic angular momentum (right) coupling curves for the lowest five electronic states of CaO, where $SO_1(X-a)$, $SO_2(A'-b)$, $SO_3(a-A')$, $SO_4(b-a)$, $SO_{1A}(A-a)$, $L_{y1}(X-A')$, $L_{y1A}(A-A')$, and $L_3(a-b)$ are defined in equations 10 and 24 of Khalil et al. (2012).

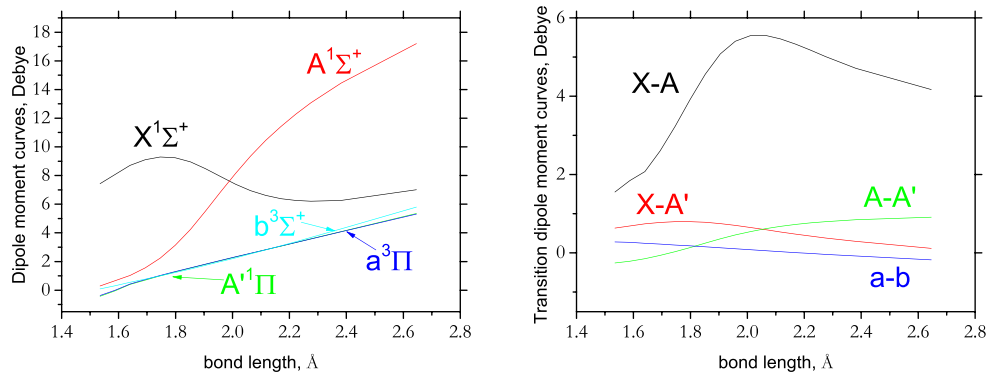

Figure 3. Ab initio dipole moment curves for the lowest five electronic states of CaO [Khalil et al. 2011; Leonard (private communication)]: permanent dipoles (left); transition dipoles (right).

to the first excited state of Ca, Ca(^{3}P), although this also involves avoided crossings in most cases. This asymptote lies 15 200 cm^{-1} (1.88 eV) higher than the lowest dissociation channel. We used the experimental dissociation value 4.11± 0.07 eV of Irvin & Dagdigian (1980) to set the dissociation asymptote of the $a\,^3\Pi$ relative to the minimum of the ground electronic state, while the next dissociation channel O(^{3}P)+Ca(^{3}P) was fixed to the value 4.1 + 1.88 = 5.99 eV. This value can be compared to the D_e value of 6.13 eV (MRCI+Q) by Khalil et al. (2011). The corresponding estimates of D_e(O(^{3}P)+Ca(^{1}S)) from the literature are 4.049 eV (CCSD(T)/cc-pCVQZ) by Iron, Oren & Martin (2003), 3.29 eV (MRCI+Q) (Khalil et al. 2011) 4.05 eV±0.07 (empirical D_0) and 3.081 eV (deperturbative D_0) due to Field (1974). Our zero-point energy is 364.675 cm^{-1} (=0.045 eV).

It is technically easier, at least initially, to do empirical refinement by fitting to energies rather than transition frequencies. To do this, we built a set of experimental energies from different sources as follows. The energy term values corresponding to the $A'\,^1\Pi$, $a\,^3\Pi$, $b\,^3\Sigma^+$ states were taken directly from Norman et al. (1989) and Baldwin & Field (1990b). Additional $X\,^1\Sigma^+$ and $A'\,^1\Pi$ energies were derived from the transition frequencies reported by Focsa et al. (2000) (supplementary material) using combination differences. We also initially used a large set of experimentally derived term values of the $A\,^1\Sigma^+$ (v = 0–5), $a\,^3\Pi$ (v = 6, 9, 12) and $A'\,^1\Pi$ (v = 7, 13) vibronic bands, all with $J \leq 60$ from van Groenendael et al. (2005). After a preliminary refinement of the *ab initio* curves to this set, our prediction had significantly improved and we could confidently start working directly with the experimental frequencies from the supplementary material by van Groenendael et al. (2005) (kindly provided by one of the authors). This material is a more extensive set of actual experimental emission frequencies ranging from J = 0 up to J = 118, i.e. even beyond J = 60 reported in their paper. All transitions are assigned J and parity (rigorous quantum 'numbers') as well as vibronic states labels ($A\,^1\Sigma^+$, v = 0–5). Some transitions from the resonance regions are represented in this material by two or three entries with identical assignment. These extra lines appear due to the intensity stealing caused by the resonances of closely lying states (in this case highly vibrationally excited $a\,^3\Pi$ and $A'\,^1\Pi$). Despite the fact that resonances make the modelling much more challenging, they provide a unique opportunity of accessing energies from the dark electronic states, which otherwise are unaccessible or difficult to observe.

Using these data and relying on van Groenendael et al's rigorous quantum numbers (J and parity), we have reconstructed the upper state energies associated with these bands by combining their experimental $A\,^1\Sigma^+$–$X\,^1\Sigma^+$ transitions (including the resonance ones) with 'our' experimentally derived energies of the (lower) $X\,^1\Sigma^+$ state. Most of the upper state energies were supported by 6–10 transitions and all energy levels characterized by only a single transitions were omitted from our analysis, thus confirming the correct assignment of their Js and parities. The $A\,^1\Sigma^+$ state ro-vibronic energy levels were obtained as an average of the corresponding upper states energy levels, which resulted in 630 levels including 250 new ones in addition to the set reported by van Groenendael et al. (2005).

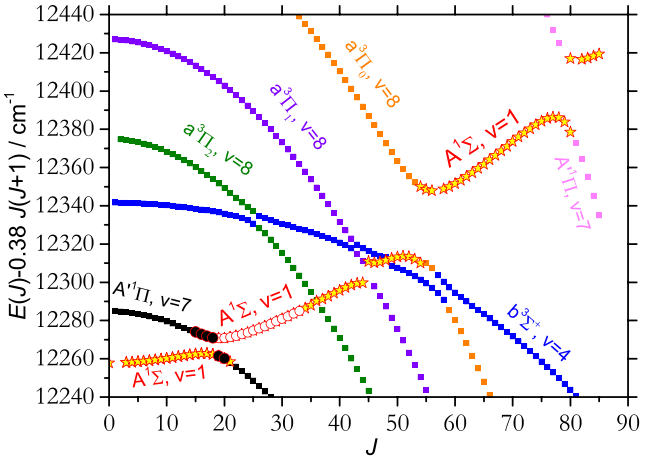

Figure 4. Reduced energy term values of CaO in the region of the $A\,^1\Sigma^+$ ($v = 1$) vibronic band: filled and empty circles represent the term values assigned by van Groenendael et al. (2005) to $A'\,^1\Pi$ ($v = 7$) and $A\,^1\Sigma^+$ ($v = 1$), respectively. Stars are the new term values assigned to $A\,^1\Sigma^+$ ($v = 1$) and filled triangles are term values from van Groenendael et al. (2005) assigned here to $A'\,^1\Pi$ ($v = 7$). Squares represent the calculated DUO levels.

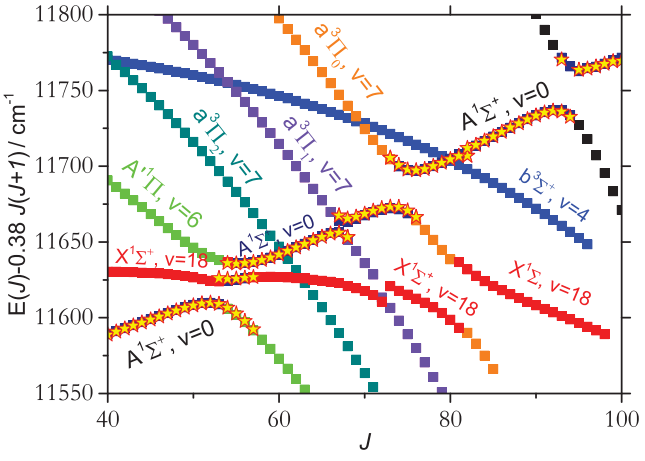

Figure 5. Reduced energy term values of CaO in the region of the $A\,^1\Sigma^+$ ($v = 0$) vibronic band: Squares represent the calculated term values and stars show the experimental energies derived using the experimental frequency wavenumbers reported by van Groenendael et al. (2005) (new for $J > 60$).

It should be noted that we could not find any transitions associated with the $a\,^3\Pi$ ($v = 6$) vibronic band as well with the $J = 38$, 39, $v = 9$ ($a\,^3\Pi$) levels in these data. Therefore they were not included into our fitting set.

Last but not least, a set of experimentally derived energies were extracted from the experimental work by Hultin & Lagerqvist (1950), where the $A\,^1\Sigma^+$–$X\,^1\Sigma^+$ system was analysed. Most of these transition wavenumbers, which are reported with an uncertainty of >0.01 cm^{-1}, are outdated by the more accurate data of van Groenendael et al. (2005), except those involving the (6, 3) and some of (5, 2) vibrational bands. Using these transitions together with 'our' experimentally derived $X\,^1\Sigma^+$-state energy levels, we were able to extend our fitting set by about 30 term values from the ($A\,^1\Sigma^+$, $v = 6$) vibronic band.

The ro-vibronic assignment (both using rigorous and approximate quantum labels) of the experimental energies/frequencies is crucial in the fits. At the first step, we had to use the assignment provided by van Groenendael et al. (2005). However after initial fits we could already rely on the assignment suggested by our DUO model, which is based on the largest basis set contributions (i.e. largest expansion coefficient). It turned out, however, that our assignments differ at high J from those by van Groenendael et al. (2005) in one important aspect related to the behaviour of resonating vibronic states at and after their crossings (in terms of J progression). This is illustrated in Fig. 4, where a network of the ro-vibronic progression as a function of J from the region of the vibronic state $A\,^1\Sigma^+$ ($v = 1$) is shown. The circles indicate the assignment by van Groenendael et al. (2005) [levels for $J = 20$–34 assigned as ($A'\,^1\Pi$, $v = 7$)] and stars and triangles represent our assignment [all levels for $J = 0$–85 assigned as ($A\,^1\Sigma^+$, $v = 1$), except five crossing states assigned as ($A'\,^1\Pi$, $v = 7$)]. In fact, the latter is more logical as the strongest transitions should belong to the $A\,^1\Sigma^+$–$X\,^1\Sigma^+$ band across all J except perhaps in the crossing regions. This indicates the limitations of the effective rotational Hamiltonian models, which most likely hindered van Groenendael et al's analysis of this vibronic progression for $J > 34$ and was not reported in their paper.

We also found similar cases where other vibronic states cross the $A\,^1\Sigma^+$ $v = 0$–5 progressions: according to the effective Hamiltonian results (van Groenendael et al. 2005), the $A\,^1\Sigma^+$ progressions tend to switch either to $a\,^3\Pi$ or $A'\,^1\Pi$ when they cross. This contrasts with our picture, which places most of the transitions from this system in the strong $A\,^1\Sigma^+$–$X\,^1\Sigma^+$ band, except for those resonance states that appear to be due to the intensity stealing ($X\,^1\Sigma^+$, $a\,^3\Pi$, and $A'\,^1\Pi$). This also applies to our newly derived energies above $J = 60$, as can be seen in Fig. 5. Therefore our fits are based on our assignment which we believe to be reliable.

As mentioned above, the positive effect of the resonances is that they provide access to other vibronic bands otherwise not visible to the experiment. Especially valuable cases are when more than two states cross which results in transitions from dark bands as well. As an illustration, Fig. 5 shows the resonance region where three vibronic states ($A\,^1\Sigma^+$, $v = 1$), ($A'\,^1\Pi$, $v = 6$) and $X\,^1\Sigma^+$ $v = 18$ meet at $J = 54$–57 and all three states are represented experimentally. The theoretical data here represent our best model after the refinement. As one can see, the DUO calculations provide not just qualitatively but also quantitatively correct description of the resonance. It is reassuring that even the shapes of the J progression of the both dark vibronic states ($A'\,^1\Pi$, $v = 6$, green squares) and ($X\,^1\Sigma^+$, $v = 18$, red squares) agree with the corresponding progressions formed by the experimental levels (stars). Again, this is a unique situation when due to intensity stealing we get access to a highly excited (e.g. $v = 18$) region of the $X\,^1\Sigma^+$ PEC; this is especially valuable for high-temperature applications.

Our complete energy set consists of 2204 term values covering the rotational excitations up to $J = 118$. At the final stage of the refinement we could include the original experimental transition wavenumbers from Hultin & Lagerqvist (1950), van Groenendael et al. (2005) and Focsa et al. (2000). Such a combined treatment was also used in our AlO work (Patrascu et al. 2014). Our final fit optimized all *ab initio* curves from Khalil et al. (2011), including five PECs, six SOCs, and three EAMCs but excluding the electronic angular momenta L^2 curves. The latter are effectively embedded into the corresponding refined PECs. In the refinements of the *ab initio* SOCs and EAMCs, we used the morphing procedure explained by Patrascu et al. (2014). Most of these curves remained very similar to the *ab initio* ones (the morphing factor is close to 1), except EAMCs

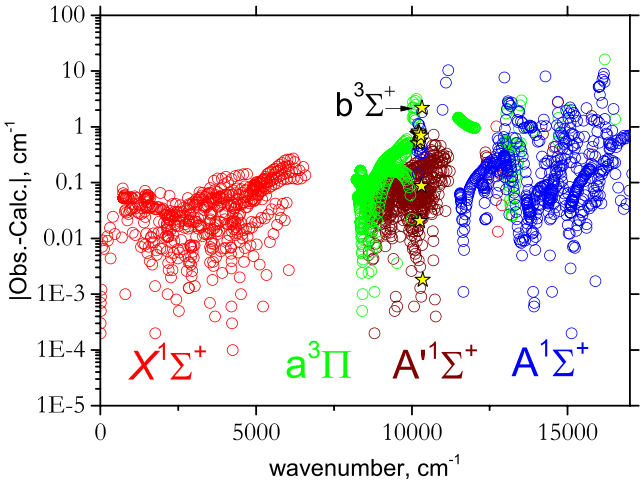

Figure 6. Accuracy of the fit: the absolute values of the residuals between the experimentally derived (obs.) and calculated (calc.) energy term values for each electronic states are shown.

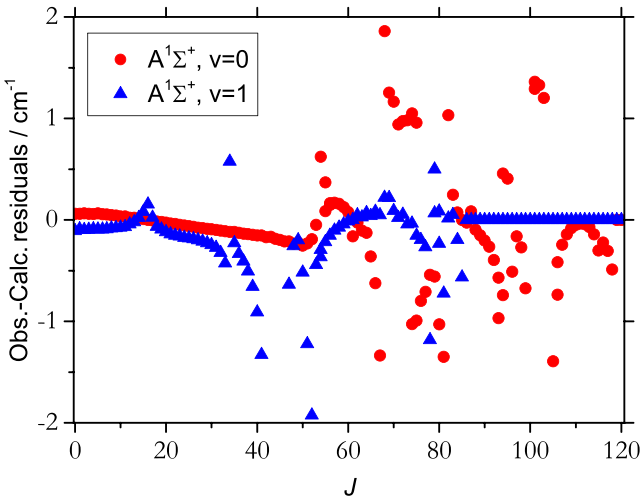

Figure 7. Obs.-calc. residuals for the ($A\,^1\Sigma^+$, $v = 0$) and ($A\,^1\Sigma^+$, $v = 1$) ro-vibronic energy levels showing the influence of the resonances.

L_{y1A} and L_{y3} (see Fig. 2), which are scaled by the factors 0.13 and −0.36, respectively.

The $b\,^3\Sigma^+$ state has a very limited experimental description, only the state $v = 1$ with $J = 14$–25 were characterized by Baldwin & Field (1990b), which is clearly not sufficient for an unambiguous determination of the corresponding PEC. We have represented the *ab initio* PEC (Khalil et al. 2011) analytically using an extended Morse oscillator function (Lee et al. 1999), where the dissociation value was changed to agree with the common value of $D_e = 5.99$ eV (relative to $X\,^1\Sigma^+$) and the T_e and r_e values were refined by keeping all other parameters from the Morse exponent unchanged. Due to the limited data, our results represent only a possible solution for this state.

Fig. 6 illustrates the accuracy of the fit. The root-mean-squares error for all experimental energies up to $J = 118$ is 0.40 cm^{-1}, (0.07 cm^{-1} for $X\,^1\Sigma^+$, 0.15 cm^{-1} for $A'\,^1\Pi$, 0.43 for $a\,^3\Pi$, 0.8 for $b\,^3\Sigma^+$, and 0.60 cm^{-1} for $A\,^1\Sigma^+$).

It should be noted that we could not resolve all resonances in the $A\,^1\Sigma^+$–$X\,^1\Sigma^+$ system, see Fig. 7. In some cases, the residuals in the resonance region are up to 1–2 cm^{-1}. We did not want to push the fit too strongly by introducing more parameters because we were not completely confident of the current representation of experimental data at the high-energy region. For example, the $b\,^3\Sigma^+$ state is one of the important players (see Fig. 5), but is clearly undersampled. Besides some of our objects already appear to be overfitted, which could affect the accuracy of prediction for high J. Despite these relatively small numbers of outliers, we find that our model performs exceptionally well especially for $X\,^1\Sigma^+$, $A'\,^1\Pi$, and $a\,^3\Pi$. Although our level of accuracy is not as high as that of effective Hamiltonian models, our extrapolations for higher v and J are likely to be much more reliable. However the high residuals in the resonance regions indicate that more work is needed in the future.

Table 2. Partition function parameters (with T in K) for CaO, see equation (1).

Parameter	Value
a_0	−3.766 046 4541
a_1	35.388 475 4545
a_2	−117.516 177 4390
a_3	215.912 921 4690
a_4	−241.034 570 6670
a_5	173.082 675 3920
a_6	−81.706 320 6245
a_7	25.207 016 7715
a_8	−4.889 591 4087
a_9	0.540 868 9698
a_{10}	−0.026 003 0674

We could also compare our theoretical energies to the 'observed' $a\,^3\Pi$ ($v = 6$) term values reported by van Groenendael et al. (2005) (see their table 1) and omitted from our analysis due to absence of the associated experimental evidence. We have found that our prediction is systematically off the 'observed' values of van Groenendael et al. (2005) by between 0.95 and 1.47 cm^{-1}, which could indicate artefacts in our model due to resonances it does not fully account for.

Our assignments of the experimental states and experimental transitions can be found in the supplementary material to this paper as part of the complete list of experimental energies and frequency wavenumbers used in the fit, together with the corresponding obs.-calc. residuals. In some cases of strongly resonating states, our assignment (based on the largest contribution from the basis set expansions) may become ambiguous due to equivalent contributions from resonating basis set components and lead to, for example, duplicate quantum labels. It can also fail for very high vibrational ($v \sim 20$) and rotational ($J > 100$) excitations when the basis set functions are strongly mixed. Therefore in these and some other cases, the assignment is not well defined and should be used with caution.

4 LINE LIST

For the final line list production with DUO, all potential energy and coupling curves were mapped on a grid of 501 equidistant points. This input is given in the supplementary material which allows these curves to be extracted for other purposes than running DUO.

The line list was generated using the refined PECs, SOCs, EAMCs, and *ab initio* dipole and transition dipole moment curves. It contains 28 418 064 transitions between states covering $J = 0 \ldots 221$ and the wavenumber range 0–20 000 cm^{-1}, with the lower and upper state energies ranging up to 20 000 and 35 000 cm^{-1},

Table 3. Extract from the state file for CaO. i: State counting number. $\tilde{E}$: State energy in cm^{-1}. g: State degeneracy. $+/-$: Total parity. e/f: rotationless-parity. v: State vibrational quantum number. Λ: Projection of the electronic angular momentum. Σ: Projection of the electronic spin. Ω: $\Omega = \Lambda + \Sigma$, projection of the total angular momentum. Full table is available from http://cdsarc.u-strasbg.fr/cgi-bin/VizieR?-source=J/MNRAS/xxx/yy.

i	$\tilde{E}$	g	J	$+/-$	e/f	State	v	Λ	Σ	Ω
1	0.000 000	1	0	+	f	X1Sigma+	0	0	0	0
2	722.452 270	1	0	+	f	X1Sigma+	1	0	0	0
3	1435.257 802	1	0	+	f	X1Sigma+	2	0	0	0
4	2138.509 986	1	0	+	f	X1Sigma+	3	0	0	0
5	2832.313 497	1	0	+	f	X1Sigma+	4	0	0	0
6	3516.781 758	1	0	+	f	X1Sigma+	5	0	0	0
7	4192.036 586	1	0	+	f	X1Sigma+	6	0	0	0
8	4858.206 860	1	0	+	f	X1Sigma+	7	0	0	0
9	5515.427 402	1	0	+	f	X1Sigma+	8	0	0	0
10	6163.838 078	1	0	+	f	X1Sigma+	9	0	0	0
11	6803.582 280	1	0	+	f	X1Sigma+	10	0	0	0
12	7434.805 019	1	0	+	f	X1Sigma+	11	0	0	0
13	8057.647 658	1	0	+	f	X1Sigma+	12	0	0	0
14	8352.058 886	1	0	+	f	a3Pi	0	1	−1	0
15	8672.234 580	1	0	+	f	X1Sigma+	13	0	0	0
16	8891.506 388	1	0	+	f	a3Pi	1	1	−1	0
17	9278.622 853	1	0	+	f	X1Sigma+	14	0	0	0
18	9424.671 614	1	0	+	f	a3Pi	2	1	−1	0
19	9876.485 742	1	0	+	f	X1Sigma+	15	0	0	0
20	9952.328 458	1	0	+	f	a3Pi	3	1	−1	0
21	10 457.945 342	1	0	+	f	X1Sigma+	16	0	0	0
22	10 482.722 422	1	0	+	f	a3Pi	4	1	−1	0
23	10 983.490 378	1	0	+	f	a3Pi	5	1	−1	0
24	11 055.566 757	1	0	+	f	X1Sigma+	17	0	0	0
25	11 488.371 123	1	0	+	f	a3Pi	6	1	−1	0
26	11 550.470 240	1	0	+	f	A1Sigma+	0	0	0	0
27	11 630.899 954	1	0	+	f	X1Sigma+	18	0	0	0
28	11 998.949 002	1	0	+	f	a3Pi	7	1	−1	0
29	12 199.329 740	1	0	+	f	X1Sigma+	19	0	0	0
30	12 257.881 985	1	0	+	f	A1Sigma+	1	0	0	0
31	12 501.179 666	1	0	+	f	a3Pi	8	1	−1	0
32	12 761.226 866	1	0	+	f	X1Sigma+	20	0	0	0
33	12 960.097 091	1	0	+	f	A1Sigma+	2	0	0	0
34	13 002.600 726	1	0	+	f	a3Pi	9	1	−1	0
35	13 316.141 667	1	0	+	f	X1Sigma+	21	0	0	0
36	13 484.091 690	1	0	+	f	a3Pi	10	1	−1	0
37	13 675.102 575	1	0	+	f	A1Sigma+	3	0	0	0
38	13 864.261 534	1	0	+	f	X1Sigma+	22	0	0	0

respectively, from the lowest five electronic states with the vibrational excitations up to $v = 80$ for $X\,^1\Sigma^+$ and 50 for the other states. For the sake of completeness, the partition function was evaluated using an energy set containing 130 660 levels covering rotational excitations up to $J_{\max} = 400$.

The line list is divided into an energy file and a transitions file. This is done using the standard ExoMol format (Tennyson, Hill & Yurchenko 2013) based on the method originally developed for the BT2 line list by Barber et al. (2006). Extracts from the CaO line list are given in Tables 3 and 4. The full line list can be downloaded from the CDS, via ftp://cdsarc.u-strasbg.fr/pub/cats/J/MNRAS/xxx/yy, or http://cdsarc.u-strasbg.fr/viz-bin/qcat?J/MNRAS//xxx/yy. The line lists and partition function together with auxiliary data including the potential parameters and dipole moment functions, as well as the absorption spectrum given in cross-section format (Hill, Yurchenko & Tennyson 2013), can all be obtained also from www.exomol.com.

As a potentially more accurate alternative, we provide an energy file where some theoretical energies are replaced with their experimental counterparts, where available, following a similar approach used by Harris et al. (2008), Barber et al. (2014) and Paulose et al. (2015). By taking the advantage of the two-file structure of our line lists, this approach improves the frequencies without affecting the intensities. It guarantees the exact reproduction of the experimental frequencies (within the experimental error) when both upper and lower state energies are replaced. However a potential drawback is the loss of the consistency of the data due to the lack of the experimental information. We leave the choice between the pure theoretical and the hybrid energy files to the user.

4.1 Partition function

We used the computed energies to generate partition function values of CaO for a large range of temperatures. Fig. 8 compares our partition function with that of Sauval & Tatum (1984). The agreement below 5000 K is very good. The differences above this temperature may well be due to our neglect of higher lying electronic

Table 4. Extract from the transitions file for CaO. f: Upper state counting number; i: Lower state counting number; A_{fi}: Einstein-A coefficient in s^{-1}; $\tilde{\nu}_{fi}$: transition wavenumber in cm^{-1}. Full table is available from http://cdsarc.u-strasbg.fr/cgi-bin/VizieR?-source=J/MNRAS/xxx/yy.

f	i	A_{fi}	$\tilde{\nu}_{fi}$
10 571	10 884	9.5518E-06	120.241 863
21 053	21 375	1.9515E-05	120.242 886
8726	9672	1.8658E-04	120.243 522
11 655	11 950	5.0065E-06	120.243 733
93 209	93 967	5.7055E-03	120.244 192
2228	3175	7.3226E-07	120.244 564
46 727	46 432	1.0599E-04	120.244 658
44 436	44 774	1.4626E-04	120.245 583
29 037	28 723	1.8052E-04	120.245 669
4458	4805	1.0431E-08	120.246 396
69 313	68 434	5.0531E-06	120.248 178
22 640	22 985	1.1281E-07	120.248 891
57 027	56 721	7.1064E-06	120.250 180
15 224	15 547	1.9505E-05	120.250 711
6779	6477	5.0457E-04	120.251 564
46 942	47 278	3.5870E-04	120.252 807
18 700	17 749	1.8354E-03	120.255 243
42 535	42 205	2.0975E-04	120.257 381
86 554	86 842	6.9691E-05	120.259 492
14 843	15 190	2.0376E-04	120.259 971
49 206	48 911	8.7081E-05	120.260 231
17 728	18 060	1.4899E-04	120.260 340
31 636	31 977	8.7497E-04	120.260 929

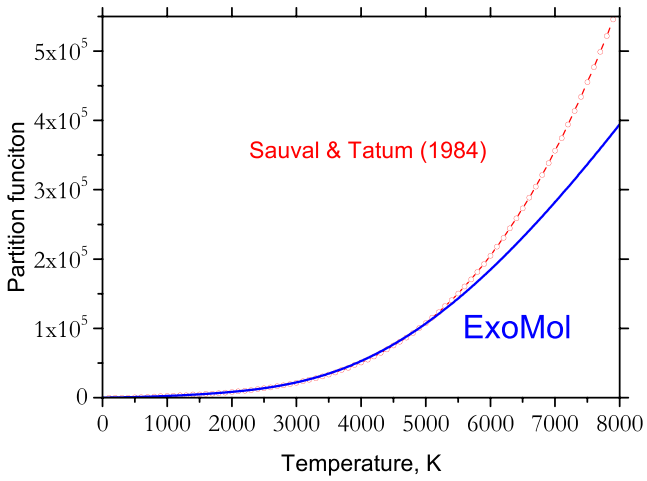

Figure 8. Partition functions of CaO as a function of temperature.

states, although assumptions in the methodology used by Sauval & Tatum (1984) may also contribute. Similarly, we obtain very good agreement with the partition function given by CDMS (not shown) (Müller et al. 2005), which only considers temperatures up to 500 K.

Following Vidler & Tennyson (2000), we represent our partition function using the functional form

$$\log_{10} Q(T) = \sum_{n=0}^{10} a_n [\log_{10} T]^n, \quad (1)$$

where the fitting parameters a_n are given in Table 2, which reproduce the partition function in Fig. 8 for entire region below 8000 K with the relative root-mean-square (rms) error of 3.6 per cent.

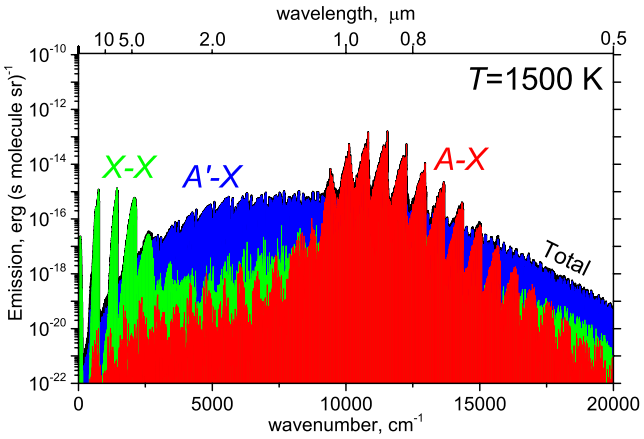

Figure 9. Emission ($T = 1500$ K) cross-sections (Gaussian profile, HWHM $= 1$ cm^{-1}) of CaO showing the three strongest dipole allowed electronic bands of CaO. The total spectrum is in the background as indicated by the black outline.

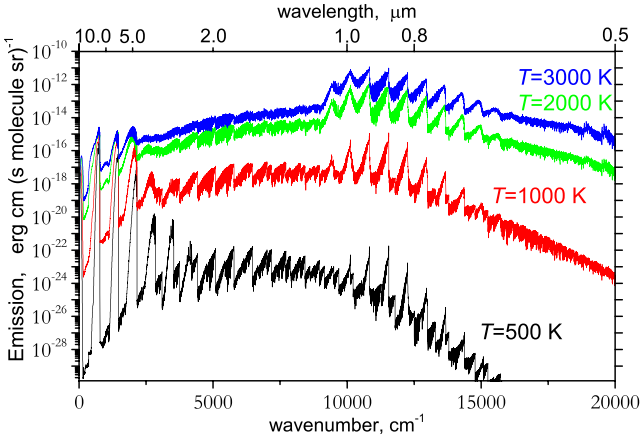

Figure 10. Temperature dependence of the emission spectra of CaO (Gaussian profile, HWHM $= 1$ cm^{-1}).

4.2 Examples of spectra

Fig. 9 gives an overview of the CaO spectrum and illustrates the contributions from each of the five bands. A notable feature of this figure is strength of all the bands in the system: several orders of magnitude stronger than is typical of molecular transition intensities. This can be attributed to the large charge separation in the $X\,^1\Sigma^+$ state of CaO, which is often represented by chemists as $Ca^{2+}O^{2-}$, the variation of this separation with geometry and the different nature of the excited states of CaO. All this means that the dipoles, which are shown in Fig. 3, are all large. Fig. 10 illustrates the strong temperature dependence of the spectra of molecular CaO.

In order to test the quality of our theoretical line list, we present a number of comparisons with previous works. Fig. 11 compares a rotational spectrum of CaO at $T = 298$ K computed using our line list with the spectrum given in the CDMS data base (Müller et al. 2005). The agreement is very good: our spectrum is slightly stronger which is a reflection of the slightly larger equilibrium $X\,^1\Sigma^+$ state dipole moment predicted by Khalil et al. (2012) than the (unpublished) calculations used by CDMS.

Fig. 12 compares an $A'\,^1\Pi - X\,^1\Sigma^+$ band emission spectrum, simulated here and from the experiment by Focsa et al. (2000). Fig. 13 illustrates the emission spectrum of $A\,^1\Sigma^+ - X\,^1\Sigma^+$ band of CaO

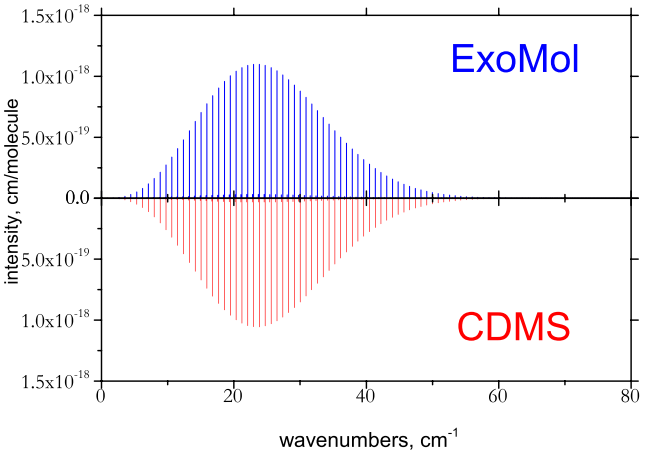

Figure 11. Comparison with the CDMS rotational band at $T = 298$ K.

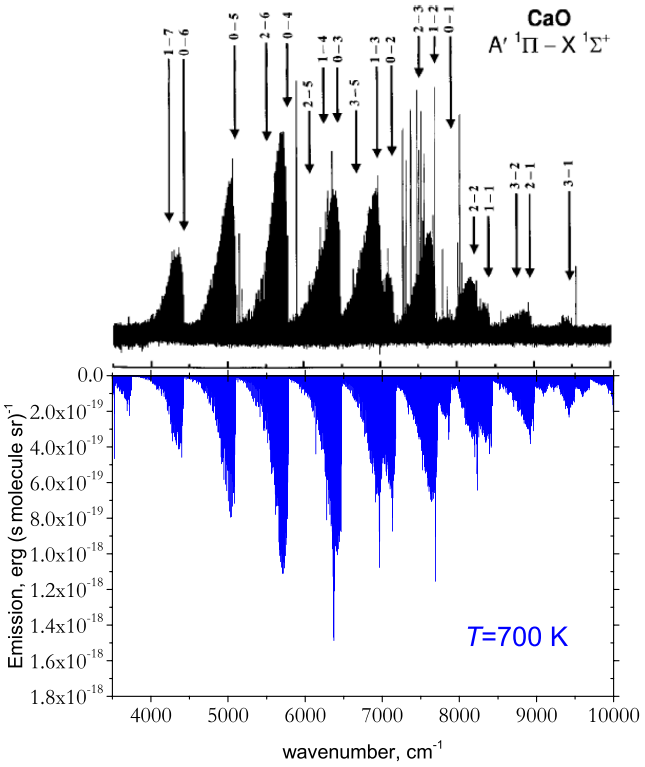

Figure 12. Comparison with experiment (Focsa et al. 2000): $T = 700$ K emission with the Doppler profile.

simulated at $T = 2000$ K using a Gaussian line profile with the half width at half-maximum (HWHM) of 1 cm^{-1}.

4.3 Lifetimes

Excited-state lifetimes, where measured, provide an independent check on our Einstein coefficients. Plane & Nien (1991) measured an average emission lifetime for the ($A\,^1\Sigma^+$, $v = 6$) vibronic state as $\tau = 149 \pm 11$ ns for an unspecified distribution of J levels. We obtain $\tau = 111$ ns for the ($J = 20$, $A\,^1\Sigma^+$, $v = 6$) and $\tau = 137$ ns for the ($J = 40$, $A\,^1\Sigma^+$, $v = 6$) levels. Given the difficulty of making a precise comparison, this represents good agreement.

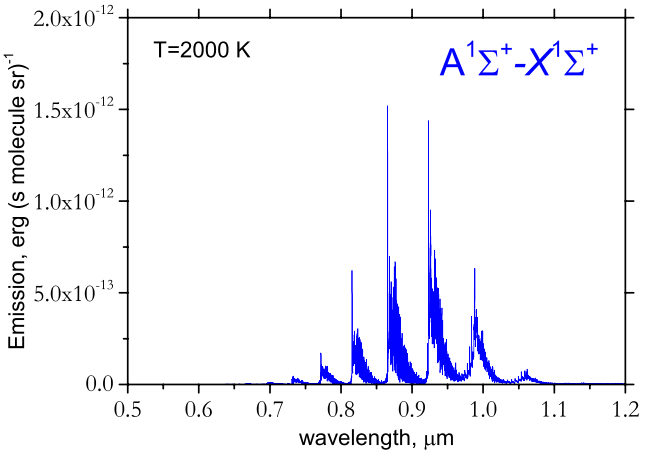

Figure 13. Emission spectrum of CaO at $T = 2000$ K, $A\,^1\Sigma^+ – X\,^1\Sigma^+$ band (Gaussian profile, HWHM = 1 cm^{-1}).

5 CONCLUSIONS

We present a comprehensive line list for calcium oxide, CaO. This line list can be downloaded from the CDS, via ftp://cdsarc.u-strasbg.fr/pub/cats/J/MNRAS/, or http://cdsarc.u-strasbg.fr/viz-bin/qcat?J/MNRAS/, or from www.exomol.com. CaO is one of a number of molecules which may be observable constituents of hot, rocky exoplanets. The ExoMol project has already provided linelists for a number of other, similar molecules including MgH and CaH (Yadin et al. 2012), SiO (Barton, Yurchenko & Tennyson 2013), NaCl and KCl (Barton et al. 2014), AlO (Patrascu et al. 2015), ScH (Lodi et al. 2015) and NaH (Rivlin et al. 2015). A number of other potentially important species, including VO (McKemmish, Yurchenko & Tennyson, in preparation), TiO, TiH, NiH and CrH (Gorman, Yurchenko & Tennyson, in preparation), are currently being studied. The ExoMol data base is also currently being upgraded to provide more extensive lists of molecular properties including pressure broadening, lifetimes and Landé g-factors; details of this will be given elsewhere (Tennyson et al. 2016b).

Using our refined model, we could re-assign vibronic labels for a large portion of the CaO transitions and levels given by van Groenendael et al. (2005) for $J \leq 60$, and also assign their transitions with $J = 60$–118. This is a reassuring illustration of the quality of our model and its ability to correctly (at least in most cases) describe the perturbations of the $A\,^1\Sigma^+$ states due interactions with other vibronic bands.

ACKNOWLEDGEMENTS

We thank C. Leonard for the *ab initio* curves and P. Bernath for the experimental line list. This work was supported by the ERC under the Advanced Investigator Project 267219 and made use of the DiRAC@Darwin, DiRAC@COSMOS HPC cluster and Emerald CfI cluster. DiRAC is the UK HPC facility for particle physics, astrophysics and cosmology and is supported by STFC and BIS. The authors would like to acknowledge the work presented here made use of the EMERALD high performance computing facility provided via the Centre for Innovation (CfI). The CfI is formed from the universities of Bristol, Oxford, Southampton and UCL in partnership with STFC Rutherford Appleton Laboratory. We also acknowledge the networking support by the COST Action CM1405 MOLIM.

REFERENCES

Baldwin D. P., Field R. W., 1989, J. Mol. Spectrosc., 133, 90
Baldwin D. P., Field R. W., 1990a, J. Mol. Spectrosc., 139, 68
Baldwin D. P., Field R. W., 1990b, J. Mol. Spectrosc., 139, 77
Baldwin D. P., Norman J. B., Soltz R. A., Sur A., Field R. W., 1990, J. Mol. Spectrosc., 139, 39
Barber R. J., Tennyson J., Harris G. J., Tolchenov R. N., 2006, MNRAS, 368, 1087
Barber R. J., Strange J. K., Hill C., Polyansky O. L., Mellau G. C., Yurchenko S. N., Tennyson J., 2014, MNRAS, 437, 1828
Barton E. J., Yurchenko S. N., Tennyson J., 2013, MNRAS, 434, 1469
Barton E. J., Chiu C., Golpayegani S., Yurchenko S. N., Tennyson J., Frohman D. J., Bernath P. F., 2014, MNRAS, 442, 1821
Blom C. E., Hedderich H. G., 1988, Chem. Phys. Lett., 145, 143
Brewer L., Hauge R., 1968, J. Mol. Spectrosc., 25, 330
Brodersen P.-H., 1932, Z. Phys., 79, 613
Castan T., Menou K., 2011, ApJ, 743, L36
Child C. D., 1911, Phys. Rev., 32, 0492
Drowart J., Verhaegen G., Exsteen G., 1964, T. Faraday Soc., 60, 1920
Field R. W., 1974, J. Chem. Phys., 60, 2400
Field R. W., Capelle G. A., Jones C. R., 1975, J. Mol. Spectrosc., 54, 156
Focsa C., Poclet A., Pinchemel B., Le Roy R. J., Bernath P. F., 2000, J. Mol. Spectrosc., 203, 330
Guenther E. W. et al., 2011, A&A, 525, A24
Harris G. J., Larner F. C., Tennyson J., Kaminsky B. M., Pavlenko Y. V., Jones H. R. A., 2008, MNRAS, 390, 143
Hedderich H. G., Blom C. E., 1989, J. Chem. Phys., 90, 4660
Hill C., Yurchenko S. N., Tennyson J., 2013, Icarus, 226, 1673
Hocking W. H., Pearson E. F., Creswell R. A., Winnewisser G., 1978, J. Chem. Phys., 68, 1128
Hocking W. H., Winnewisser G., Churchwell E., Percival J., 1979, A&A, 75, 268
Hultin M., Lagerqvist A., 1950, Ark. Fys., 166, 190
Hultin M., Lagerqvist A., 1951, Ark. Fys., 2, 471
Iron M. A., Oren M., Martin J. M. L., 2003, Mol. Phys., 101, 1345
Irvin J. A., Dagdigian P. J., 1980, J. Chem. Phys., 73, 176
Ito Y., Ikoma M., Kawahara H., Nagahara H., Kawashima Y., Nakamoto T., 2015, ApJ, 801, 144
Khalil H., Brites V., Le Quere F., Leonard C., 2011, Chem. Phys., 386, 50
Khalil H., Le Quere F., Brites V., Leonard C., 2012, J. Mol. Spectrosc., 271, 1
Lagerqvist A., 1954, Ark. Fys., 8, 83
Lagerqvist A., Huldt L., 1954a, Z. Nat.forsch. A, 9, 991
Lagerqvist A., Huldt L., 1954b, Ark. Fys., 8, 427
Lagerqvist A., Nilsson N. E. L., Barrow R. F., 1957, Ark. Fys., 12, 543
Lee E. G., Seto J. Y., Hirao T., Bernath P. F., Le Roy R. J., 1999, J. Mol. Spectrosc., 194, 197
Leger A. et al., 2009, A&A, 506, 287
Leitzinger M. et al., 2011, PASP, 59, 1472
Lodi L., Yurchenko S. N., Tennyson J., 2015, Mol. Phys., 113, 1559
Marks R. F., Schweda H. S., Gottscho R. A., Field R. W., 1982, J. Chem. Phys., 76, 4689
Müller H. S. P., Schlöder F., Stutzki J., Winnewisser G., 2005, J. Molec. Struct., 742, 215
Norman J. B., Cross K. J., Schweda H. S., Polak M., Field R. W., 1989, Mol. Phys., 66, 235
Patrascu A. T., Hill C., Tennyson J., Yurchenko S. N., 2014, J. Chem. Phys., 141, 144312
Patrascu A. T., Tennyson J., Yurchenko S. N., 2015, MNRAS, 449, 3613
Paulose G., Barton E. J., Yurchenko S. N., Tennyson J., 2015, MNRAS, 454, 1931
Plane J. M. C., Nien C. F., 1991, J. Chem. Soc. Faraday Trans., 87, 677
Rivlin T., Lodi L., Yurchenko S. N., Tennyson J., Le Roy R. J., 2015, MNRAS, 451, 5153
Rouan D., Deeg H. J., Demangeon O., Samuel B., Cavarroc C., Fegley B., Leger A., 2011, ApJ, 741, L30
Sakamoto S., White G. J., Kawaguchi K., Ohishi M., Usuda K. S., Hasegawa T., 1998, MNRAS, 301, 872
Samuel B., Leconte J., Rouan D., Forget F., Leger A., Schneider J., 2014, A&A, 563, A103
Sauval A. J., Tatum J. B., 1984, ApJS, 56, 193
Schaefer L., Lodders K., Fegley B. Jr, 2012, ApJ, 755, 41
Svyatkin I. A., Kuznetsova L. A., Kuzyakov Y. Y., 1980a, J. Quant. Spectrosc. Radiat. Transfer, 23, 307
Svyatkin I. A., Kuznetsova L. A., Kuzyakov Y. Y., 1980b, J. Quant. Spectrosc. Radiat. Transfer, 24, 25
Tennyson J., Yurchenko S. N., 2012, MNRAS, 425, 21
Tennyson J., Hill C., Yurchenko S. N., 2013, in AIP Conf. Proc. Vol. 1545, in Gillaspy J. D., Weise W. L., Podpaly Y. A., eds, Eighth International Conference on Atomic and Molecular Data and their Applications: ICAMDATA-2012. Am. Inst. Phys., New York, p. 186
Tennyson J., Lodi L., McKemmish L. K., Yurchenko S. N., 2016a, J. Phys. B: At. Mol. Opt. Phys., topical Review
Tennyson J. et al., 2016b, J. Mol. Spectrosc.
Tinetti G. et al., 2012, Exp. Astron., 34, 311
Tinetti G. et al., 2016, Exp. Astron., 40, 329
van Groenendael A., Tudorie M., Focsa C., Pinchemel B., Bernath P. F., 2005, J. Mol. Spectrosc., 234, 255
Vidler M., Tennyson J., 2000, J. Chem. Phys., 113, 9766
Winn J. N. et al., 2011, ApJ, 737, L18
Yadin B., Vaness T., Conti P., Hill C., Yurchenko S. N., Tennyson J., 2012, MNRAS, 425, 34
Yurchenko S. N., Lodi L., Tennyson J., Stolyarov A. V., 2016, Comput. Phys. Commun.

SUPPORTING INFORMATION

Additional Supporting Information may be found in the online version of this article:

– A Duo-input file used to produce the line list for CaO containing all the curves, PECs, SOCc, EAMS (both refined and ab initio) and ab initio DMCs and TDMCs.
– Partition function of CaO
– A complete fitting list of the experimentally derived energies, used in the refinements including the corresponding residuals.
– Experimental and theoretical wavenumbers from [05VaTuFo, 50HuLa] assigned by Duo.
– Empirical PECs, SOCs, and EAMCs used in intensity calculations.

In addition: **Table 3.** Extract from the state file for CaO.
Table 4. Extract from the transitions file for CaO. (http://www.mnras.oxfordjournals.org/lookup/suppl/doi:10.1093/mnras/stv2858/-/DC1).

Please note: Oxford University Press is not responsible for the content or functionality of any supporting materials supplied by the authors. Any queries (other than missing material) should be directed to the corresponding author for the article.

This paper has been typeset from a TEX/LATEX file prepared by the author.